European Journal of Neuroscience, Vol. 17, pp. 113–118, 2003

Neuronal representation of odourants in the olfactory bulb of *Xenopus laevis* tadpoles

Dirk Czesnik, Wolfgang Rössler, Friedrich Kirchner, Arne Gennerich and Detlev Schild
Physiologisches Institut, Universität Göttingen, Humboldtallee 23, 37073 Göttingen, Germany

Keywords: calcium imaging, odour representation, olfactory bulb

Abstract

When an odourant enters the nose, olfactory receptor neurons (ORNs) convey information about it to the olfactory bulb (OB), where this information is processed and where the first central representations of the odourant are generated. In this paper we show how odourants are represented by ensembles of OB neurons, in particular mitral cells (MCs) which are the output neurons of the OB. We were able to demonstrate for the first time that the intracellular calcium concentrations ($[Ca^{2+}]_i$) in the somata of these neurons undergo specific changes and that different stimuli are represented by different neuronal $[Ca^{2+}]_i$ patterns. The similarity of patterns was assessed by cross-correlation analysis. We further show that noradrenaline (NA), which is reported to be involved in olfactory memory formation and to modulate synaptic transmission at dendrodendritic synapses in the OB, profoundly changes the representation of odourants at the level of MCs.

Introduction

The CNS processes environmental stimuli in a distributed, parallel fashion. Realtime observation of stimulus-induced spatio-temporal stimulus representations at cellular resolution is a challenging task because it requires controlled natural stimulation alongside the simultaneous monitoring of brain tissue activities at the microscopic level.

We have developed a new preparation that exposes several stages of the olfactory system to imaging with Ca^{2+}-sensitive dyes. Most of our knowledge about the physiological behaviour of olfactory bulb (OB) neurons is based on studies of single OB neurons (Matsumoto & Hildebrand, 1981; Mori, 1987; Imamura *et al*., 1992; Mori & Yoshihara, 1995; Mori *et al*., 1999; Xu *et al*., 2000), on voltage-sensitive dye imaging of the surface of the OB (Kauer, 1988; Cinelli *et al*., 1995; Kauer & White, 2001; Wachowiak & Cohen, 2001; Spors & Grinvald, 2002) and on imaging neural processes in glomeruli (Friedrich & Korsching, 1997; Joerges *et al*., 1997; Friedrich & Korsching, 1998; Keller *et al*., 1998; Fuss & Korsching, 2001). However, measuring the cellular representation of odourants by ensembles of output neurons of the OB has remained illusive until now.

To accomplish this goal, we developed a tissue slice preparation which includes the olfactory epithelium, the olfactory bulb and most of the brain. In this preparation (i) olfactory receptor neurons can be monitored by patch-clamp and imaging techniques, (ii) receptor axons retain their natural connection to the olfactory bulb, (iii) the olfactory bulb is sufficiently translucent to allow CCD imaging or laser scanning of the OB, and (iv) the OB receives efferent input from other centres of the CNS.

In this paper we set out to image the activation of olfactory bulb neurons following stimulation with odourants. We obtained first insights into the spatiotemporal patterns of odourant-induced activation as well as their GABAergic and noradrenergic modulation.

Correspondence: Dr D. Schild, as above.
E-mail: dschild@gwdg.de

Received 16 May 2002, revised 15 October 2002, accepted 17 October 2002

doi:10.1046/j.1460-9568.2003.02448.x

Materials and methods

Calcium-imaging of olfactory bulb neurons and odourant stimulation

Tadpoles (stages 51–53, after Nieuwkoop & Faber, 1956) were anaesthetized in a mixture of ice and water for at least 5 min, and a block of tissue containing the olfactory mucosae, olfactory nerves and the entire brain down to the brainstem was cut out. The tissue was glued to the stage of a vibroslicer (VT 1000, Leica, Bensheim, Germany), and only the dorsal surface of the olfactory bulbs was sliced off. The olfactory mucosae and the rest of the brain were left intact. The nose–brain preparation was transferred to a recording chamber, and incubated for 1 h at room temperature in 200 μL of frog saline containing (in mM) NaCl, 98; KCl, 2; $CaCl_2$, 1; $MgCl_2$, 2; glucose, 5; pyruvate-Na, 5; HEPES, 10; and Fura 2/AM, 0.05, pH = 7.8. All chemicals except Fura-2/AM (Molecular Probes, Leiden, Netherlands) were purchased from Sigma (Deisenhofen, Germany). After incubation, the tissue was rinsed with saline, glued into the recording chamber using 5% low melting point agarose (Amresco, Agarose type II, no. 210–815), covered with saline and viewed with Nomarski optics (Axioskop 2, Zeiss, Göttingen, Germany). Preparations were rinsed with saline for at least 20 min under a constant bath flow at a rate of 550 μL/min in the recording setup. For calcium imaging, fluorescence image pairs F340/F380 (alternating excitation at 340 and 380 nm; emission >505 nm) of the olfactory bulb were taken using a frame-transfer, back-illuminated CCD camera (16 bits/pixel, Micromax; Visitron, München, Germany) and a custom-built monochromator. Images were acquired at 200 or 500 ms exposure time per image using the commercial image acquisition software Winview (Visitron). The image evaluation software was written in the lab. The $[Ca^{2+}]_i$ responses of mitral and granule cells were represented as ratio images, whereby the mean values of the autofluorescence of unstained slices were taken into account (220 and 300/pixel at 340 nm and 380 nm, respectively). The background-corrected ratio R of the fluorescence images excited at 340 and 380 nm (F340 and F380) was taken as an estimate of $[Ca^{2+}]_i$. Spatial

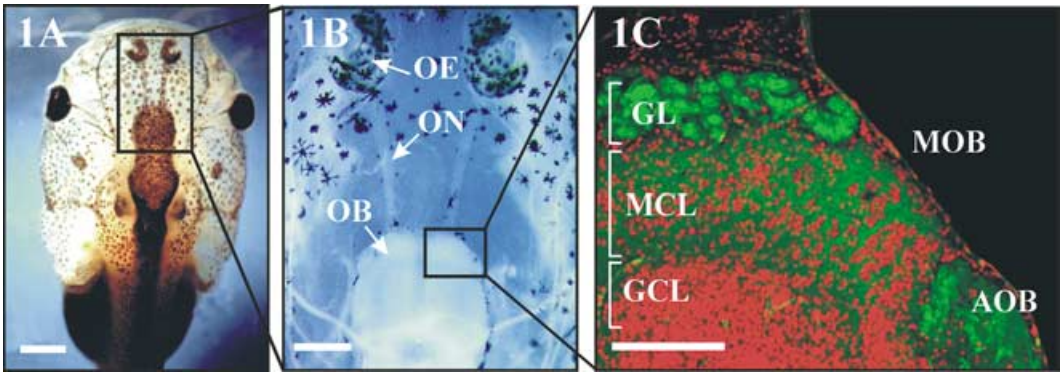

FIG. 1. Brain slice preparation including the olfactory epithelia (OE), the olfactory bulbs (OB) and the brain of *Xenopus laevis* tadpoles. (A) *Xenopus laevis* tadpole. The black rectangle indicates the block of tissue that was cut out for the experiments. (B) Higher magnification of the anterior part of the nose–brain preparation showing the OB with the top sliced open, the olfactory epithelia, and the olfactory nerves (ON). (C) OB double labelled with an antibody to synaptophysin (green) and propidium iodide (red) showing the glomerular layer (GL) and the organization of cell nuclei in the mitral (MCL) and granule (GCL) cell layers. MOB, main OB; AOB, accessory OB. Scale bars, 1.5 mm (A), 750 μm (B), 200 μM (C).

$[Ca^{2+}]_i$ patterns were revealed from ratio images R (Fig. 2B), and temporal changes in $[Ca^{2+}]_i$ patterns, i.e. $\Delta[Ca^{2+}]_i(t)$, from $\Delta R(t) = R(t) - R_o$, with R_o being the prestimulus control ratio image. In this context, the magnitudes $[Ca^{2+}]_i$, R, $\Delta[Ca^{2+}]_i$ and ΔR are understood as images and thus depend on the pixel coordinates (x,y), e.g. $R = R(x,y)$.

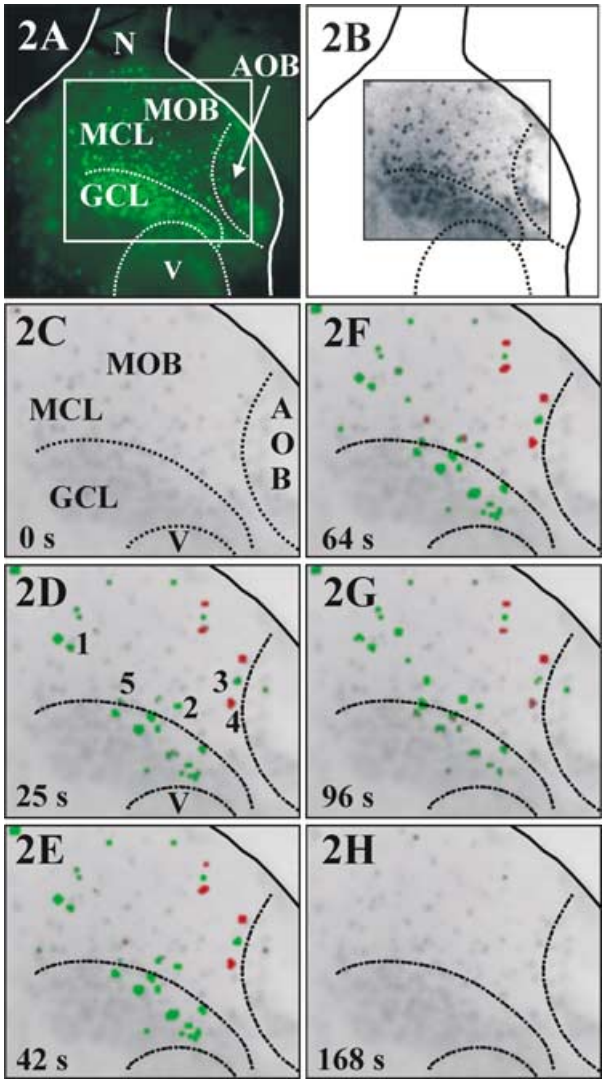

The similarity of two responses, e.g. $\Delta R_1(x,y)$ and $\Delta R_2(x,y)$, at a certain time was obtained by calculating the cross-correlation coefficient (Papoulis, 1991) r, $r = \Sigma[\Delta R_1(x,y)\ \Delta R_2(x,y)]/(\sigma_1\ \sigma_2)$, where the sum is taken over the pixels, and σ_1 and σ_2 are the standard deviations of $\Delta R_1(x,y)$ and $\Delta R_2(x,y)$, respectively. The value r is 0 in the case of uncorrelated images, it is 1 for identical images and -1 if one image of an image pair is the negative of the other one.

For odourant stimulation, we used either single amino acids (L-form) or a mixture of 15 L-amino acids (glycine, alanine, serine, threonine, cysteine, valine, leucine, isoleucine, methionine, proline, arginine, lysine, histidine, phenylalanine and tryptophan, all from Sigma-Aldrich, each at a concentration of 100 μM). Odorant stimuli were applied directly into the ipsilateral mucosa by gravity feed from a storage syringe through a funnel drug applicator (Schild, 1985) at a flow of 250 μL/min. The tip of the applicator was placed above the mucosa. Odorants were pipetted directly into the funnel without stopping the flow. The flow at the funnel outlet was constant. Fast removal of odourants was provided by a fast additional bath flow (550 μL/min) and suction through a syringe needle placed close to the mucosa and behind the stimulus applicator to ensure that odourant molecules were removed rapidly by the fast bath stream. Suction was adjusted to balance bath flow through the funnel applicator and the fast bath flow. The minimum interstimulus interval was 5 min.

Results

We recorded odourant-induced neuronal activity patterns in the novel slice preparation shown in Fig. 1. The layering of the *Xenopus* OB (Nezlin & Schild, 2000) is shown in Fig. 1C. Calcium imaging with Fura-2 revealed the cell bodies of neurons in the OB slice (Fig. 2A and

FIG. 2. Imaging of changes in somatic $[Ca^{2+}]_i$ in OB neurons reveals spatial and temporal patterns of cells activated in response to stimulation with natural odourants. (A) Fluorescence of neuronal cell bodies (F380) loaded with Fura-2. The white box indicates the region imaged. N, nerve layer, MOB, main OB; MCL, mitral cell layer; GCL, granule cell layer; V, ventricle; AOB, accessory OB (for comparison, see Fig. 1C). The dotted lines indicate the borders of the mitral and granule cell layers, the ventricle, and the AOB. (B) Ratio image R of the selected region of interest. (C–H) $[Ca^{2+}]_i$ activation patterns in response to stimulation with methionine (100 μM) at different times (in s) before, during and after odourant application. The stimulus was applied at $t = 22$ s for 7 s. The delta ratio, $\Delta R(t) = R(t) - R_o$, highlights the changes in $[Ca^{2+}]_i$. Green spots indicate neuronal cell bodies showing an increase in $[Ca^{2+}]_i$ whereas red indicates a decrease in $[Ca^{2+}]_i$. For better orientation, the response patterns are superimposed on the first ratio image.

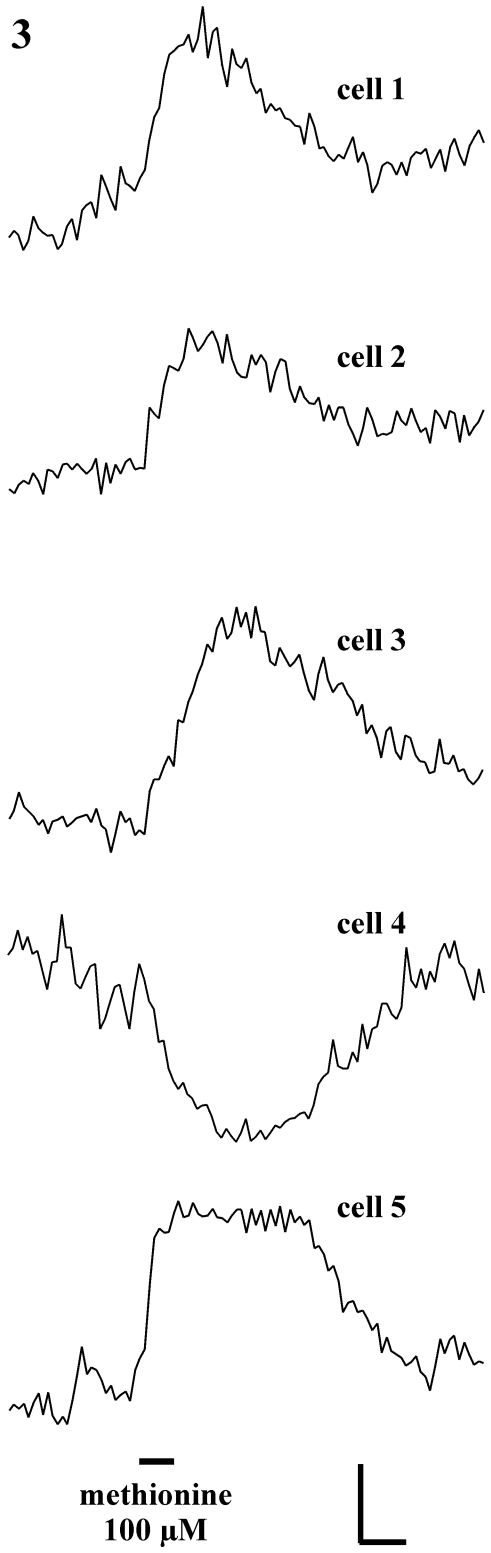

FIG. 3. Time courses of increasing or decreasing $[Ca^{2+}]_i$ respones imaged in single neuronal cell bodies within the mitral cell layer. (A–C and E) Examples of an increase in $[Ca^{2+}]_i$. (D) A cell responding with a decrease in $[Ca^{2+}]_i$. The corresponding cell bodies are indicated in Fig. 2D. The horizontal bar indicates the time and duration of methionine application (100 µM). Scale bars, $t = 10$ s, $\Delta R = 0.05$.

B), and stimulation of the olfactory mucosa with odourants clearly affected the $[Ca^{2+}]_i$ pattern of OB neurons (Fig. 2C–H). We show spatial $[Ca^{2+}]_i$ patterns as ratio images R (Fig. 2B), and temporal changes in $[Ca^{2+}]_i$ patterns, i.e. $\Delta[Ca^{2+}]_i(t)$, as $\Delta R(t) = R(t) - R_o$, where R_o is the prestimulus control ratio image. Responses of increased or decreased $[Ca^{2+}]_i$ are shown in green or red, respectively, superimposed on the first ratio image in grey scale as background. In this representation nonresponsive somata appear dark grey while the somata of responding cells are shown as coloured spots.

In the example shown, stimulation with methionine (100 µM) induced an increase in $[Ca^{2+}]_i$ in a specific ensemble of neurons (green) and a decrease in others (red). Most neurons were unaffected (dark grey).

The time courses of $[Ca^{2+}]_i$ of individual neurons were excitatory or inhibitory as shown in Fig. 3 for the neurons indicated in Fig. 2D. The earliest $[Ca^{2+}]_i$ changes following stimulation occurred with a delay of 0.8 s. The excitatory or inhibitory odour-induced $[Ca^{2+}]_i$ changes were always reversible. Some recordings showed superimposed oscillations around 0.4 Hz. Interestingly, the odourant-induced increases or decreases in $[Ca^{2+}]_i$ were almost on the same order of magnitude. Statistics on 132 responding neurons gave $\Delta R = 0.103 \pm 0.03$ (excitation, $n = 81$) and $\Delta R = -0.057 \pm 0.021$ (inhibition, $n = 51$), respectively.

Repeated application of the same stimulus gave very similar temporal patterns (Fig. 4, cells 1, 2 and 3); some cells underwent fluctuations that were uncorrelated with the odourant applications (Fig. 4, cell 4). Thus, the response patterns were similar but not identical (Fig. 5A and B).

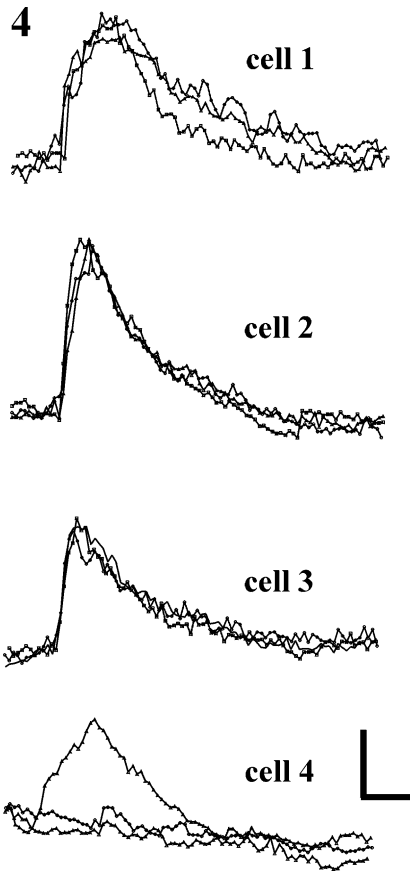

FIG. 4. Responses to repeated olfactory stimulation with the same odour (methionine, 100 µM). Similar $[Ca^{2+}]_i$ time courses of cell 1, 2 and 3. Cell 4 showed a large $[Ca^{2+}]_i$ excursion in one of three trials. This $[Ca^{2+}]_i$ transient started prior to stimulus application and was thus uncorrelated to it. Scale bars, $t = 10$ s, $\Delta R = 0.1$.

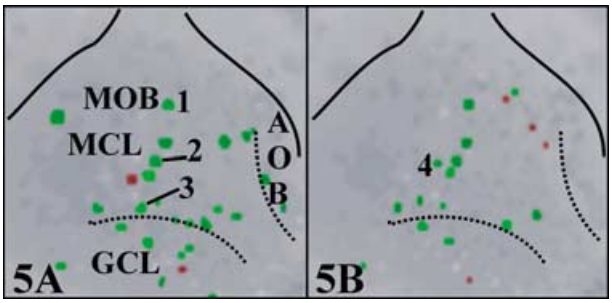

FIG. 5.

Different stimuli gave rise to different response patterns (Fig. 6), whereby several neurons were clearly involved in coding more than one odourant. In some cases neurons responded antagonistically to different odourants, e.g. excitatory to one odourant and inhibitory to another. The *r*-values of the image pairs in Fig. 6 were $r = 0.55$ (met, his), 0.21 (met, leu), 0.19 (met, arg), 0.08 (his, arg), 0.26 (his, leu), 0.5 (leu, arg), respectively. The activation patterns in response to methionine and histidine were thus more similar to each other ($r = 0.55$) than, e.g., the patterns in response to arginine and to methionine ($r = 0.19$), or arginine and histidine ($r = 0.08$).

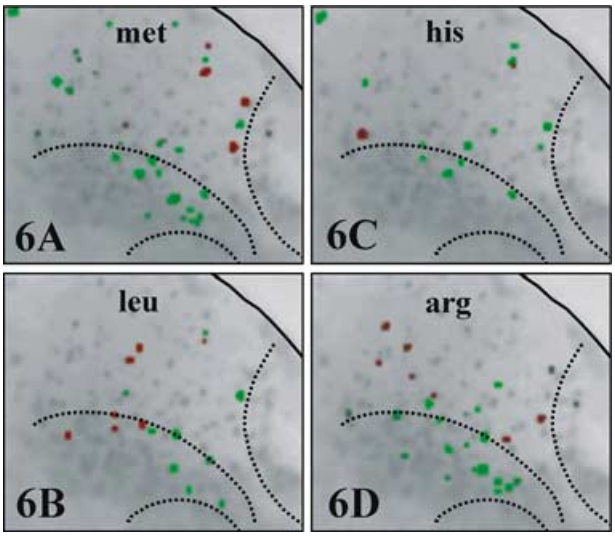

FIG. 6.

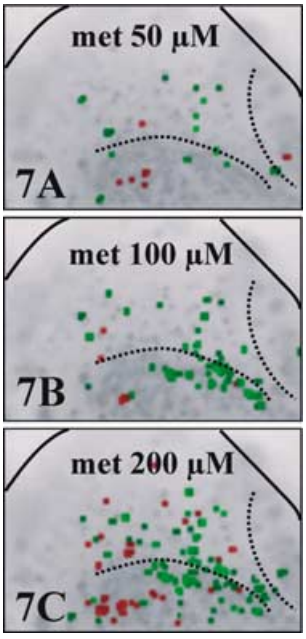

FIG. 7.

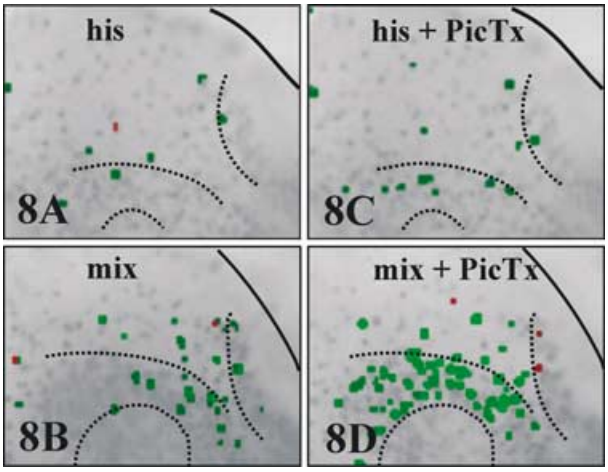

FIG. 8.

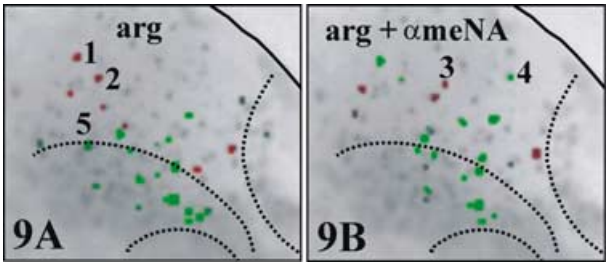

FIG. 9.

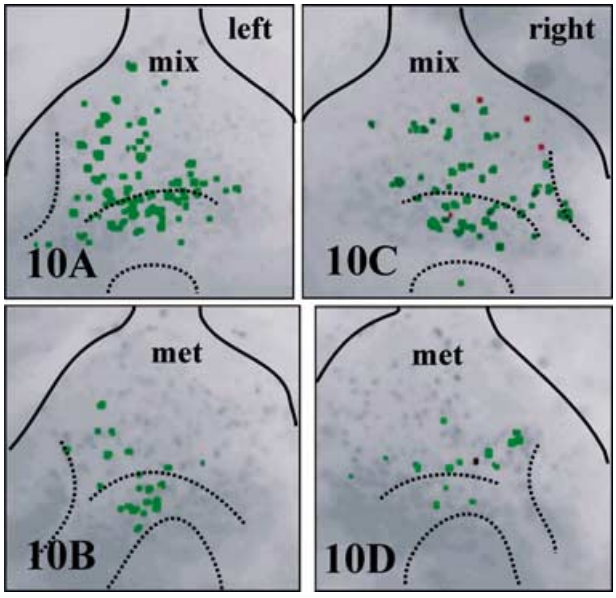

FIG. 10.

Odourant-induced activity patterns showed a marked concentration dependence (Fig. 7). The standard odourant concentration used was 100 μM (e.g. Figure 7B). At a concentration of 50 μM (Fig. 7A, methionine, 50 μM), fewer cells, especially fewer granule cells, were activated. On the other side, a higher concentration led to a general broadening of the pattern, but also to an increase in inhibitory responses (Fig. 7C, methionine, 200 μM).

Feedback and lateral inhibition in the OB via reciprocal synapses is mediated by GABA (Jahr & Nicoll, 1982a, b; Mori, 1987). It was therefore not unexpected that a marked change in odourant-induced activation patterns by blocking $GABA_A$ channels with picrotoxin (PicTx) was found (Fig. 8, $r_{his/his+PicTx} = 0.16$, $r_{mix/mix+PicTx} = 0.104$). As NA strongly affects feedback inhibition (Jahr & Nicoll, 1982a, b; Czesnik *et al*., 2001) we were particularly interested in the modulation of $[Ca_{2+}]_i$ patterns by NA. If odourants were applied while an α_2-agonist, clonidine (200 nM) or α-methyl-noradrenaline (αMeNA; 10 μM; Ruffolo *et al*., 1994), was in the bath, the response patterns deviated considerably from those with no α_2-agonists added (tested with arginine in 14 slices, with histidine in 15 slices and with methionine in 16 slices). Figure 9 shows a typical example where arginine was used as stimulus. Some cells were inhibited by the control stimulus and disinhibited by the same stimulus after αMeNA was added to the bath (e.g. cell 1 or 2 in Fig. 9). Other neurons that were unaffected by the control stimulation were either inhibited (e.g. cell 3 in Fig. 9B) or excited (e.g. cell 4 in Fig. 9B) by the same stimulus after application of αMeNA. Finally, some cells that were excited by the control stimulation became unaffected after αMeNA or clonidine application (e.g. cell 5 in Fig. 9A). The overall effect of αMeNA led to a pattern that was virtually uncorrelated with the control stimulus-induced pattern ($r = -0.03$).

As a last point we tried to verify the presumed symmetry of odourant responses in the left and right OB of the same slice. The resulting odourant-induced patterns showed some similarity but were never perfectly symmetrical (Fig. 10). We were unable to determine whether this was due to a slightly oblique sectioning of the slices or to a real asymmetry of the bulbs.

Discussion

In this study we imaged large ensembles of OB neurons. The information provided by these measurements is different from and complementary to that obtained by recent recordings of glomerular activation patterns (Friedrich & Korsching, 1997; Joerges *et al*., 1997; Friedrich & Korsching, 1998; Fuss & Korsching, 2001; Wachowiak & Cohen, 2001; Spors & Grinvald, 2002). In higher vertebrates, olfactory receptor neurons (ORNs) of a particular class express one type of olfactory receptor (OR) and the ORNs of the same class project to the same glomerulum. Though this scheme has as yet not been confirmed in lower vertebrates, it may be assumed that glomerular activation patterns reflect the specificities of ORNs mapped onto the glomerular layer, i.e. they reflect the specificity-differentiated input to the OB. Glomeruli then couple to mitral cells (MCs) through the primary dendrites of MCs and through a complex network of interneuronal connections. In addition, MC activation patterns can be modulated indirectly by efferent innervation through interneurons. MC activation patterns are thus the result of the signal processing in the OB and reflect the spatial output pattern of the OB.

We measured patterns of somatic $[Ca^{2+}]_i$ rather than voltage or spiking patterns, because $[Ca^{2+}]_i$ dyes are presently superior to voltage-sensitive dyes in terms of toxicity and recording time, signal-to-noise ratio, ratiometric evaluation and applicability in tissue slices. The exact dynamics of the somatic $[Ca^{2+}]_i$ signals depend on a number of partly unknown parameters such as localization and types of calcium channels (Bischofberger & Schild, 1995), $[Ca^{2+}]_i$-release mechanisms (Geiling & Schild, 1996) and Ca^{2+}-buffering (Neher, 1995). Experimental (Smetter *et al*., 1999; Peterlin *et al*., 2000; Charpak *et al*., 2001) as well as theoretical (Engel *et al*., 1999) work suggests that the $[Ca^{2+}]_i$ signal of OB neurons follows membrane potential and neuronal activity, albeit in a nonlinear and complex manner which needs to be studied in the future. The spatial information on how neuronal activity changes is thus reflected by the spatial $[Ca^{2+}]_i$ pattern. Our imaging data clearly show the following three features of OB coding.

Differences between spatiotemporal patterns

The activity patterns induced by different stimuli in the same slice can easily be distinguished from each other and are similar (although not identical) in the left and right OB. The cross-correlation coefficient of different patterns is a useful though rather coarse measure of similarity. More refined measures/descriptors that characterize patterns and their differences in more detail should be tried in the future.

Lateral inhibition

There is a high density of reciprocal synapses between mitral cells and interneurons in the OB (Shepherd, 1996) suggesting an important role of lateral inhibition in the OB signal processing. Our data confirm this. Blocking lateral inhibition changes the OB output pattern dramatically. A response pattern induced by a certain stimulus (control) is almost uncorrelated to the corresponding pattern induced by the same stimulus but with lateral inhibition blocked. The decreased calcium level in the

FIG. 5. Responses to repeated olfactory stimulation with the same odour. (A and B) $[Ca^{2+}]_i$ activation patterns in response to two stimulations with methionine (100 μM). The time interval between the stimulations was 8 min.

FIG. 6. Olfactory stimulation with different amino acids give rise to different $[Ca^{2+}]_i$ response patterns of OB neuron somata. $[Ca^{2+}]_i$ activation pattern in response to stimulation with (A) methionine (met, 100 μM), (B) leucine (leu, 100 μM), (C) histidine (his, 100 μM) and (D), arginine (arg, 100 μM). All patterns are shown at the time of maximum activation.

FIG. 7. Olfactory stimulations of different concentrations of stimuli of the same odour lead to different patterns. (A) $[Ca^{2+}]_i$ activation patterns in response to stimulation with methionine (50 μM); (B) $[Ca^{2+}]_i$ activation patterns in response to stimulation with methionine (100 μM); (C) $[Ca^{2+}]_i$ activation patterns in response to stimulation with methionine (200 μM).

FIG. 8. The $GABA_A$ receptor antagonist picrotoxin (PicTx) alters neuronal activation patterns in response to olfactory stimulation with amino acids. (A) $[Ca^{2+}]_i$ activation pattern in response to olfactory stimulation with histidine (100 μM) before and (C) after application of PicTx (100 μM). (B) $[Ca^{2+}]_i$ activation pattern in response to a mixture of 15 amino acids (mix, 100 μM each) before and (D) after application of PicTx (100 μM). All patterns are shown at the time of maximum activation.

FIG. 9. The α_2-receptor agonists αMeNA modulates lateral inhibition of odour-induced activation in OB neurons. (A) $[Ca^{2+}]_i$ activation pattern in response to stimulation with arginine (100 μM) before and (B) after application of αMeNA (10 μM). All patterns are shown at the time of maximum activation of neurons.

FIG. 10. Olfactory stimulation of both the left and the right olfactory epithelium and resulting activity patterns in the olfactory bulbs. (A and B) Left OB, $[Ca^{2+}]_i$ activation patterns in response to stimulation with mix of amino acids (A, 100 μM) and with methionine (B, 100 μM). (C and D) Right OB, $[Ca^{2+}]_i$ activation patterns in response to stimulation with mix of amino acids (C, 100 μM) and with methionine (D, 100 μM).

two spots on the right in Fig. 7D cannot be explained right now. One could hypothesize that picrotoxin, by increasing MC activity, leads to some sort of an as yet undiscovered efferent innervation to granule cells.

Noradrenergic modulation

NA has been shown to play a crucial role in olfactory memory formation and odour learning (Brennan et al., 1990; Brennan & Keverne, 1997). Our data show a strong influence of clonidine or αMeNA upon the OB output pattern. These drugs are selective agonists of α_2-receptors, which have been shown to be localized at the MC face of some but not all reciprocal synapses of the OB (Czesnik et al., 2001). The rather complex response pattern changes upon αMeNA application (Fig. 8) are consistent with inhibition of glutamatergic synaptic transmission from MCs to granule cells (GCs), the direct effect being a decreased excitation of GCs. These, in turn, disinhibit the MCs connected to them. As α_2-agonists modulate some but not all MCs (Czesnik et al., 2001) and as GC dendrites show complex arborizations, the disinhibitory effect on MCs could be expected to be likewise complex. Moreover, the disinhibited MCs affect the activity of the interneurons they are connected to, which would render the resulting pattern changes even more complex. It was thus not surprising that α_2-agonist application led to a pattern which was virtually uncorrelated with the original pattern, induced by the same stimulus but without α_2-agonists applied.

Acknowledgements

This work was supported by SFB 406 (A12, B5) from Deutsche Forschungsgemeinschaft. We want to thank G. Federkeil und J. Kuduz for expert technical help.

Abbreviations

αMeNA, α-methyl-noradrenaline; F340 and F380, fluorescence images excited at 340 and 380 nm, respectively; GC, granule cell; MC, mitral cell; OB, olfactory bulb; ORN, olfactory receptor neuron; PicTx, picrotoxin; R, background-corrected ratio of the fluorescence images excited at 340 and 380 nm; R_o, prestimulus control ratio.

References

Bischofberger, J. & Schild, D. (1995) Different spatial patterns of $[Ca^{2+}]$ increase caused by N-and L-type Ca^{2+}-channel activation in frog olfactory bulb neurones. *J. Physiol. (Lond.)*, **487**, 305–317.

Brennan, P., Kaba, H. & Keverne, E.B. (1990) Olfactory recognition: a simple memory system. *Science*, **250**, 1223–1226.

Brennan, P.A. & Keverne, E.B. (1997) Neural mechanisms of mammalian olfactory learning. *Prog. Neurobiol.*, **51**, 457–481.

Charpak, S., Mertz, J., Beaurepaire, E., Moreaux, L. & Delaney, K. (2001) Two photon imaging of odor-evoked Ca^{2+} dynamics in dendritic compartments of rat mitral cells. *Proc. Natl Acad. USA*, **98**, 1230–1234.

Cinelli, A.R., Hamilton, K.A. & Kauer, J.S. (1995) Salamander olfactory bulb neuronal activity observed by video rate, voltage-sensitive dye imaging: III. Spatial and temporal properties of responses evoked by odorant stimulation. *J. Neurophysiol.*, **73**, 2053–2071.

Czesnik, D., Nezlin, L., Rabba, J., Mueller, B. & Schild, D. (2001) Noradrenergic modulation of calcium currents and synaptic transmission in the olfactory bulb of *Xenopus laevis* tadpoles. *Eur. J. Neurosci.*, **13**, 1093–1100.

Engel, J., Schultens, H.A. & Schild, D. (1999) Small conductance potassium channels cause an activity-dependent spike frequency adaptation and make the transfer function of neurons logarithmic. *Biophys. J.*, **76**, 1310–1319.

Friedrich, R.W. & Korsching, S.I. (1997) Combinatorial and chemotopic odorant coding in the zebrafish olfactory bulb visualized by optical imaging. *Neuron*, **18**, 737–752.

Friedrich, R.W. & Korsching, S.I. (1998) Chemotopic, combinatorial, and noncombinatorial odorant representations in the olfactory bulb revealed using a voltage-sensitive axon tracer. *J. Neurosci.*, **18**, 9977–9988.

Fuss, S.H. & Korsching, S.I. (2001) Odorant feature detection: activity mapping of structure response relationships in the zebrafish olfactory bulb. *J. Neurosci.*, **21**, 8396–8407.

Geiling, H. & Schild, D. (1996) Glutamate-mediated release of Ca^{2+} in mitral cells of the olfactory bulb. *J. Neurophysiol.*, **76**, 563–570.

Imamura, K., Mataga, N. & Mori, K. (1992) Coding of odor molecules by mitral/tufted cells in rabbit olfactory bulb. I. Aliphatic compunds. *J. Neurophysio.L*, **68**, 1986–2002.

Jahr, C.E. & Nicoll, R.A. (1982a) An intracellular analysis of dendrodendritic inhibition in the turtle *in vitro* olfactory bulb. *J. Physiol. (Lond.)*, **326**, 213–234.

Jahr, C.E. & Nicoll, R.A. (1982b) Noradrenergic modulation of dendrodendritic inhibition in the olfactory bulb. *Nature*, **297**, 227–229.

Joerges, J., Kuttner, A., Galizia, C.G. & Menzel, R. (1997) Representations of odours and odour mixtures visualized in the honeybee brain. *Nature*, **387**, 285–288.

Kauer, J.S. (1988) Real-time imaging of evoked activity in local circuits of the salamander olfactory bulb. *Nature*, **331**, 166–168.

Keller, A., Yagodin, S., Aroniadou–Anderjaska, V., Zimmer, L.A., Ennis, M., Sheppard, N.F. Jr & Shipley, M.T. (1998) Functional organization of rat olfactory bulb glomeruli revealed by optical imaging. *J. Neurosci.*, **18**, 2602–2612.

Kauer, J.S. & White, J. (2001) Imaging and coding in the olfactory system. *Annu. Rev. Neurosci.*, **24**, 963–979.

Matsumoto, S.G. & Hildebrand, J.G. (1981) Olfactory mechanims in the moth *Manduca sexta:* response charactersitics and morphology of central neurons in the antennal lobes *Proceedings R. Soc. Lond. B.*, **213**, 249–277.

Mori, K. (1987) Membrane and synaptic properties of identified neurons in the olfactory bulb. *Prog. Neurobiol.*, **29**, 275–320.

Mori, K., Nagao, H. & Yoshihara, Y. (1999) The olfactory bulb: coding and processing of odor molecule information. *Science*, **286**, 711–715.

Mori, K. & Yoshihara, Y. (1995) Molecular recognition and olfactory processing in the mammalian olfactory system. *Prog. Neurobiol.*, **45**, 585–619.

Neher, E. (1995) The use of fura-2 for estimating Ca^{2+} buffers and Ca^{2+} fluxes. *Neuropharmacology*, **34**, 1423–1442.

Nezlin, L. & Schild, D. (2000) Structure of the olfactory bulb in tadpoles of *Xenopus laevis*. *Cell. Tissue Res.*, **302**, 21–29.

Nieuwkoop, P.D. & Faber, J. (1956) *Normal Table of Xenopus Laevis* (Daudin). Elsevier-North Holland, Amsterdam.

Papoulis, A. (1991) *Probability, Random Variables and Stochastic Processes*. McGraw-Hill, New York.

Peterlin, Z.A., Kozloski, J., Mao, B.Q., Tsiola, A. & Yuste, R. (2000) Optical probing of neuronal circuits with calcium indicators. *Proc. Natl Acad. Sci. USA*, **97**, 3619–3624.

Ruffolo, R.R., Stadel, J.M. & Hieble, J.P. (1994) α-adrenoreceptors: recent developments. *Med. Res. Rev.*, **14**, 229–270.

Schild, D. (1985) A computer-controlled device for the application of odours to aquatic animals. *J. Electrophysiol. Techn.*, **12**, 71–79.

Shepherd, G.M. (1996) The dendritic spine: a multifunctional integrative unit. *J. Neurophysiol.*, **75**, 2197–2210.

Smetters, D., Majewska, A. & Yuste, R. (1999) Detecting action potentials in neuronal populations with calcium imaging. *Meth. Enzymol.*, **18**, 215–221.

Spors, H. & Grinvald, A. (2002) Spatio-temporal dynamics of odor representations in the mammalian olfactory bulb. *Neuron*, **34**, 301–315.

Wachowiak, M. & Cohen, L.B. (2001) Representation of odorants by receptor. Neuron input to the mouse olfactory bulb. *Neuron*, **32**, 723–735.

Xu, F., Greer, C.A. & Shepherd, G.M. (2000) Odor maps in the olfactory bulb. *J. Comp Neurol.*, **422**, 489–495.